



Microplastics in the western Pacific and South China Sea: Spatial variations reveal the impact of Kuroshio intrusion[☆]



Mengyang Liu^{a,b,c}, Yongcheng Ding^d, Peng Huang^{c,e}, Haowen Zheng^c, Weimin Wang^c, Hongwei Ke^c, Fajin Chen^e, Lihua Liu^f, Minggang Cai^{a,b,c,d,*}

^a State Key Laboratory of Marine Environmental Science, Xiamen University, Xiamen, 361102, China

^b Fujian Provincial Key Laboratory for Coastal Ecology and Environmental Studies, Xiamen University, Xiamen, 361102, China

^c College of Ocean and Earth Sciences, Xiamen University, Xiamen, 361102, China

^d Coastal and Ocean Management Institute, Xiamen University, Xiamen, 361102, China

^e College of Ocean and Meteorology, Guangdong Ocean University, Zhanjiang, 524088, China

^f CAS Key Laboratory of Gas Hydrate, Guangzhou Institute of Energy Conversion, Chinese Academy of Sciences, Guangzhou, 510640, China

ARTICLE INFO

Keywords:

Microplastics
Kuroshio intrusion
Oceanic transport
South China Sea
Western Pacific

ABSTRACT

Surface currents play an essential role in the worldwide distribution of microplastics in the coastal seas and open oceans. As a branch of the western boundary currents (WBCs), Kuroshio changes seawater properties and pollutant levels of the South China Sea (SCS) during its intrusion process. To study the impact of Kuroshio intrusion on microplastics, we conducted field observations on surface water from the western Pacific (WP) and SCS. Microplastic abundances in the surface water of WP ($0.02\text{--}0.10 \text{ particles m}^{-3}$) were generally lower than those in the SCS ($0.05\text{--}0.26 \text{ particles m}^{-3}$). Fragments and granules dominated their apparent characteristics, and showed spatial classifications in different areas. The abundance of fragment, granule and foam showed a similar unimodal trend, as they peaked when the Kuroshio fraction was 0.1, implying the effect of Kuroshio intrusion was a combination of the dilution and biogeochemical influence. The polymer types of microplastics, dominated by polypropylene (PP), polyethylene (PE), polyester (PES), polymethacrylate (PMA) and phenoxy resin (PR), showed complicated compositions in the northern SCS, and Kuroshio intrusion was not the dominant influencing factor. Further study is needed to discover the comprehensive effect of Kuroshio intrusion on the fate of microplastics and is expected for the whole WBC system.

1. Introduction

Plastic debris is receiving increasing concerns due to its ecotoxicological effects, such as the potential for biological ingestion, chemical persistence, high sorption capacities for persistent organic pollutants and heavy metals, and choking or starving hazards after ingestion (Sussarellu et al., 2016; Egger et al., 2020; Li et al., 2020; Chen et al., 2020). In addition, with physical forcing, UV radiation and chemical degradation, plastic debris could become fragmented and oxidized into smaller particles, reaching the microscale and nanoscale (Gigault et al., 2016; Poulain et al., 2019). Microplastics are undergoing considerable accumulation due to intense consumption and disposal, and has been detected in all marine environments, from the coastlines to the open ocean, tropical to polar regions, and the surface to the seafloor (Lebreton

et al., 2017; Mai et al., 2019; Sterl et al., 2020; Zhao et al., 2020; Xia et al., 2021).

Surface currents play an essential role in the worldwide distribution of microplastics, and they could provide dynamics on transporting particles in the coastal seas and open oceans (Lusher et al., 2015; Waller et al., 2017; Zhang et al., 2020). Buoyant plastics are prone to end up in the open ocean after long-range transport by ocean currents, and during this process, horizontal convergence works to constrain passive particles with increased retention at the surface (Schling et al., 2013; Cozar et al., 2014; Egger et al., 2020). High microplastic abundances exist in the open oceans' central areas, and especially in the North Pacific Ocean, such as the Subtropical Convergence Zone and "Garbage Patches" (Howell et al., 2012; Wichmann et al., 2019). The surrounding Asian coast is regarded as a hotspot source of microplastics, and the annual

[☆] This paper has been recommended for acceptance by Eddy Y. Zeng.

* Corresponding author. State Key Laboratory of Marine Environmental Science, Xiamen University, Xiamen, 361102, China.

E-mail address: mgc@xmu.edu.cn (M. Cai).

emissions of plastics from China and the Philippines account for 32% of the global marine load (Jambeck et al., 2015; Tang et al., 2018). However, there is a ten-hundred-fold gap between the land-based input and ocean-based inventory in microplastics (Poulain et al., 2019; Mai et al., 2020). Besides, many studies on microplastic distributions are conducted with modelling, focusing on open oceans and gyre dynamics rather than marginal seas and coastal areas (Hale et al., 2020). Such knowledge gap motivates further studies combined with field observation to investigate the fate of microplastics from the coastal to the open ocean.

In the previous studies of microplastics, researchers focused on the effect of ocean currents mainly from a dynamic physical perspective. However, it is less known about the impact of ocean currents on their biogeochemical processes (Brunner et al., 2015; Mountford and Morales Maqueda, 2019; Sterl et al., 2020). The Kuroshio Current (KC), as one of the western boundary currents (WBCs) located in the western Pacific (WP), starts from the bifurcation of the North Equatorial Current (NEC) and could merge terrestrial-sourced materials (Qiu and Miao, 2000; Imawaki et al., 2001). Besides the majority of the KC flowing out of the South China Sea (SCS) and transporting heat and materials to higher latitudes, a branch of KC intrudes into the SCS through the Luzon Strait, influencing the marginal sea's water properties, circulation and biogeochemical processes (Qiu and Chen, 2005; Nan et al., 2015; Liu et al., 2021). The unique characteristics of the SCS-WP system would facilitate better understanding the role of ocean currents on microplastics and discovering the interactions between the open oceans and the marginal seas.

Although some studies have obtained several data of microplastics in the SCS and WP, most of them focus on the coastal or insular areas, but little is known about their oceanic transport (Cai et al., 2018a,b; Pan et al., 2019; Wang et al., 2019). To investigate the influence of Kuroshio intrusion on microplastics, we presented the spatial distribution and characteristic variation of microplastics in the SCS-WP system, and

analyzed the relationship between microplastic characteristics and the Kuroshio fraction.

2. Materials and methods

2.1. Study area and hydrology

Two cruises were carried out in this study in 2017, one with the R/V *Dongfanghong II* in July and August and the second with the R/V *Kexue* in October and November. The locations, bottom depths, wind speeds and sampling dates are present in Table S1 in the Supporting Information. Temperature and salinity data of seawater were collected shipboard with a conductivity-temperature-depth (CTD) profiler. The sampling areas (Fig. 1) cover the WP, SCS and Luzon Strait. Sampling sites E130-7, E130-9, E130-12, E130-14, E130-16, F2 and N18-9 were in the WP, while the others were in the SCS.

2.2. Sampling

The microplastic samples were collected from surface seawater by a manta trawl, and the details have been described in our previous paper (Tang et al., 2018). Briefly, the trawl was deployed behind the research vessel with a mesh size of 330 µm, a height of 0.5 m, and a width of 1 m. After ensuring that all the material was in good condition, we slowly dragged the trawl from the rear of the deck until the trawl was oriented in the correct direction. The surface trawling lasted for 10 min at a relative speed of water of 3 knots at each site. The sampling volume was calculated according to the tow distance obtained with the onboard knot-meter, multiplied by the sampling time, width and averaged sampling height of the trawl. As soon as the net was towed back onto the deck, it was rinsed with seawater. The collected samples were washed into a 500 mL glass jar and fixed in 2.5% formaldehyde solution.

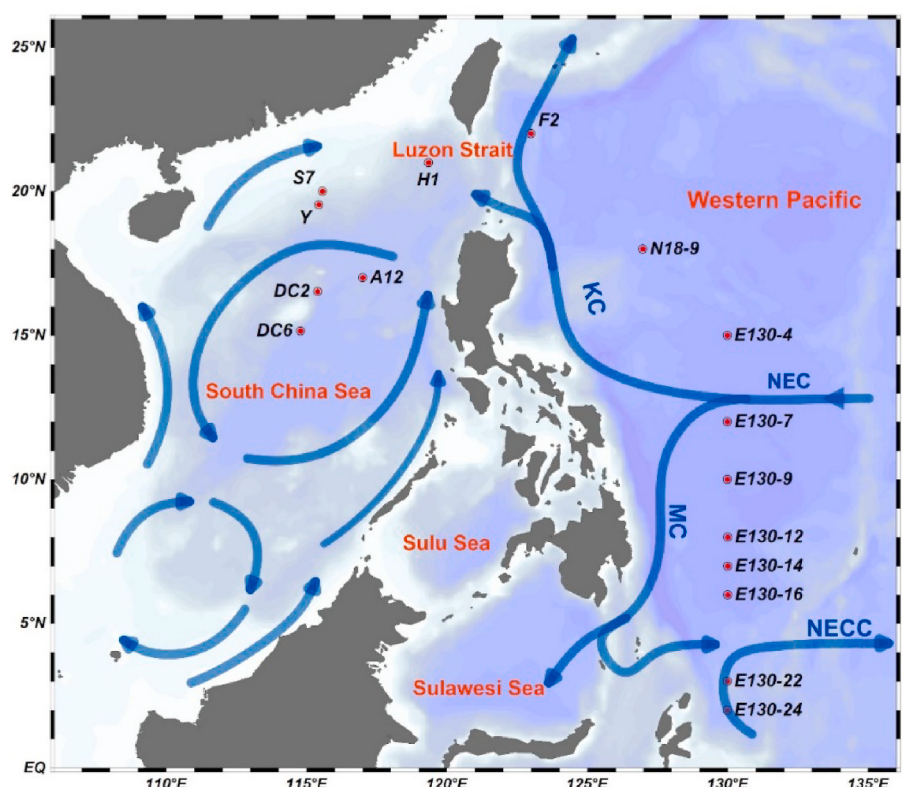


Fig. 1. Map of the sampling area and major surface ocean currents. The sampling areas covered the western Pacific, Luzon Strait and South China Sea, where the major surface currents include the North Equatorial Current (NEC), Kuroshio Current (KC), Mindanao Current (MC) and North Equatorial Counter Current (NECC).

2.3. Pretreatment and identification

The pretreatment procedures mainly included three steps: wet sieving, digestion and density separation, and these details are described in our previous paper (Cai et al., 2018a,b; Tang et al., 2018). Briefly, the samples in the glass jar were filtered through pre-cleaned stainless-steel mesh sieves (5.0 mm) and further filtered by a nylon filter (Millipore, 20 µm). Then the retentate on the filter was transferred to a beaker that contained 500 mL 30% H₂O₂. The solution was placed at 37 °C with a hotplate for 24 h for digestion, and the mouth of beaker was covered with aluminum foil with several small holes. The solution volume and velocity of the bubbles were checked from time to time until they were similar to the blank samples. After filtering the digestion solution with a nylon filter, the retentate in the beaker was repeatedly rinsed with prefiltered saturated NaCl solution (1.20 g cm⁻³) to transfer and filter in the same way. Plastic particles were separated by floatation in NaCl solution for 24 h and further collected on the filter by filtration. Finally, the filter membranes and the solid intercepting substance were stored in membrane boxes in a dark and stable room temperature environment.

Details of the observation for microplastic samples are present in Text S1. Briefly, the microplastic targets were observed, measured and counted using a stereoscopic microscope (Dino-Lite, AM4113T (R4), Taiwan) at 40× magnification. We took approximate 25–30 photos for each filter, using a “zigzag” pattern until the membrane filter being fully covered. Representative microplastic particles with high abundance, or large sizes or unique colors, as well as those considered to require identification, were selected. The sizes of microplastics were documented as the longest length of each particle, and the shapes and colors were also documented during the counting process.

For each sample, 20 particles were picked randomly for polymer type identification, and three different sections were detected for one particle. The identification of polymer type was performed with a micro-Fourier Transform Infrared Spectroscopy (micro-FTIR) (Nicolet iN10, Thermo Fisher Scientific, U.S.A.), and processed by OMNIC Picta software. The spectral range was 7800–350 cm⁻¹, with 16 scans at a resolution of 4 cm⁻¹. The instrument was stable and accurate, and it had no spectral deviation or distortion during the identification. The spectra were compared to the OMNIC polymer reference spectra library, and a sample was considered plastic only when the matching rate to a plastic component of the database was higher than 60%.

2.4. QA/QC

Sampling devices and filter meshes were cleaned with Milli-Q water before use to reduce the potential contamination, and samples were collected quickly into a glass jar and sealed onboard. The instruments used in the experiment were mainly glassy and metallic, and we rinsed all the instruments with Milli-Q water three times and then dried them before the experiments. The openings of the instruments were covered with aluminum foil to reduce air pollution, and all chemicals were filtered through a polyethersulfone membrane (Merck Millipore, 0.22 µm) to avoid particulate contaminants. Experimenters wore 100% cotton and nitrile gloves during the pretreatment and analysis procedure, and the doors and windows were kept closed during the experiment to reduce the flow of air.

During each cruise, three field blank samples were conducted on board to detect the potential contamination from the air, net, ship and lab. At the beginning of the cruise and before the trawling, field blanks were collected by rinsing the nets with distilled water without trawling, then transferred to a glass jar and treated as other samples. Field blanks of this research were 27 ± 10 particles/jar. The abundances of microplastic reported here were corrected for the field blanks. Replicate sampling was not conducted because of the time constraints and sea conditions.

2.5. Calculation and equations

To assess the degree of microplastic photo-degradation, we calculated the carbonyl index (CI) according to the FTIR spectra as equation (1):

$$\text{Carbonyl Index (CI)} = \frac{A_{C=O}}{A_{\text{ref}}} \quad (1)$$

where A_{C=O} is the absorbance at 1700–1750 cm⁻¹ for carbonyl groups (C=O), and A_{ref} is the absorbance at 1450–1500 cm⁻¹ for reference peaks (CH). The carbonyl index usually increases with the enhancing photo-degradation.

The Kuroshio fraction (R_K) is based on the in-situ observations and the conservative properties of salinity (S), which is of less seasonal variance than the temperature. R_K is estimated with a validated isopycnal model as Eq. (2) (Du et al., 2013; Wang et al., 2017; Wu et al., 2015):

$$R_K = \frac{S - S_S}{S_P - S_S} \quad (2)$$

where S_S denotes the salinity value of the central SCS water, and site DC6 is representative of this end member. S_P denotes the salinity value of the Pacific water, which is represented by the sample from site N18-9. The salinity of surface water in the northern SCS is present in Table S6. The positive value of R_K indicates a net inflow from the WP to the SCS, while a negative value indicates the opposite direction.

2.6. Data analysis

Statistical analysis, such as the significant difference test, principal component analysis and one-dimensional cluster analysis, was performed using software SPSS (version 25), and two-dimensional hierarchical cluster analysis was performed using NCSS (version 12.0.2). The significant difference test was using the Mann-Whitney *U* test and Kruskal-Wallis test, with *p* < 0.05 indicating statistical significance. The calculation, such as carbonyl index, and Kuroshio fraction (R_K) by isopycnal model, were performed using Microsoft Excel (2010). Figures were produced by software Ocean Data View (version 5.1.5), Grapher (version 15.3.339), MATLAB (version 2019a) and NCSS (version 12.0.2).

3. Results and discussion

3.1. Microplastic occurrence and characteristics

3.1.1. Abundances

Microplastics were detected at all sampling sites in the SCS and the WP. Overall, the abundance range was 0.02–0.10 particles m⁻³ (mean 0.06 ± 0.03 particles m⁻³) for samples in the surface water of WP, lower than that in the SCS (0.05–0.26 particles m⁻³, mean 0.13 ± 0.07 particles m⁻³) (Fig. 2, Table S2). The highest abundance was found at site DC2 in the open SCS, while the lowest was found at site E130-9 in the tropical WP. The abundance fluctuated significantly in the two areas, where the differences between maximum and minimum abundances were more than two orders of magnitude.

It is worth noting that there are uncertainties mainly in the sampling volume and the percentage of identified polymer. Although Manta trawling is commonly used for sampling in the ocean with the advantage of remaining in surface water except in rough water, it has turbulence and differences in submersion. It even tends to jump or skip on rough water (Schönlau et al., 2020). As the net was not consistently submerged at the same height of the frame, the estimated value would not represent its actual sampling volume. On the other hand, there are usually two recommended methods for obtaining the tow distances. One is from the relative speed of the seawater according to the onboard knot meter, and

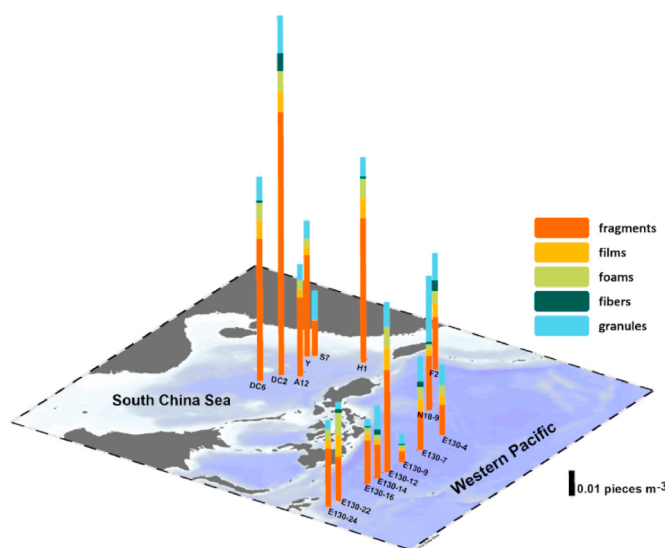


Fig. 2. The abundances and components of microplastics in the surface water from the South China Sea and western Pacific.

another is from a flow meter installed in the net mouth. According to the comparison of these two methods, these obtained tow distances are almost similar. However, the values measured with flow meter are slightly lower than that with knot meter. In that case, the sampling volume is likely to be overestimated, and the microplastic abundance would be underestimated. Besides, the quantity of particles collected with Manta net is smaller than that obtained by filtering the same surface water. There was a statistically significant difference in the weight of particles collected by different sampling methods (Green et al., 2018). Also, because the percentages of polymers identified with micro-FTIR were not same as those of the whole sample observed with the microscope, the accuracy is limited by the number of particles analyzed by micro-FTIR.

The reported microplastic abundances were of a maximum difference of 12-order magnitude in worldwide seawaters mainly due to the difference in methods (Sun et al., 2021). Here we only compared the magnitudes of our results with the reported results, rather than the detailed abundances. As shown in Table S3, abundance magnitude obtained from this study was within those from other ocean areas, such as the south Pacific Ocean ($0\text{--}0.8$ particles m^{-3}) (Eriksen et al., 2013), the north Atlantic Ocean ($0\text{--}1.16$ particles m^{-3}) (Law et al., 2014) and the Arctic Ocean ($0\text{--}1.31$ particles m^{-3}) (Lusher et al., 2015). Compared with the reported magnitudes in the neighboring marginal seas, our results were within the range of the Bohai Sea and Yellow Sea ($0.03\text{--}1.6$ particles m^{-3}) (Mai et al., 2018), as well as the Bering Sea and the Chukchi Sea ($0.018\text{--}0.31$ particles m^{-3}) (Mu et al., 2019).

3.1.2. Apparent characteristics

Five types of shapes were observed in our samples, including granule, fragment, fiber, film and foam. Granule was the most abundant in the WP and the SCS (Table S4), contributing $41 \pm 9.6\%$ and $51 \pm 3.4\%$ on average to the total microplastics in the WP and the SCS, respectively. The fragment was another dominant shape, with contributions of $33 \pm 8.5\%$ and $36 \pm 5.3\%$ in these two areas. These shapes were followed by film, fiber and foam, whose total contributions were $26 \pm 13\%$ and $13 \pm 9.2\%$ in the WP and SCS, respectively. Except film, the other shapes did not show significant differences ($p < 0.05$) between the WP and the SCS.

Seven colors were observed in this study, which are white, black, transparent, red, blue, yellow and green (Table S4). Black was the most abundant color in the WP, contributing 30% of the total abundance on average, followed by white (25%) and red (20%) colors. The proportions of blue and yellow microplastics were the lowest, contributing 2.7% and

6.1% of the total, respectively. While in the SCS, white and green microplastics were most abundant, contributing 32% and 30% of the total abundance. The proportions of blue and transparent microplastics were the lowest, contributing 1.0% and 5.5% of the total. Only the black and green were significantly different ($p < 0.05$) between the WP and the SCS. Together with the significant difference test in shape, we could infer that the apparent characteristics of microplastics from the two areas were partly similar.

To summarize the apparent characteristics of the microplastics, cluster analysis (CA) and principal component analysis (PCA) were performed on their shapes and colors. As shown in Fig. S1, the five shape types and seven colors were primarily divided into two clusters, where each cluster could be further divided into two parts. In cluster 1, one part was characterized with black color only, and another part was characterized with shapes of foam, film and fiber, and colors of blue, transparent, yellow and red. In cluster 2, the green color was classified into one group individually, while fragment, granule and the white were classified into another group. Although no obvious classification was found in terms of the color, the classification of shapes reflected the similar distribution of low-weight plastics such as foam, fiber and film. We obtained three principal components in the PCA, namely PC1, PC2 and PC3, and they explained 48% , 18% and 12% of the total variance in the apparent characteristics data matrix. As shown in Fig. S2, PC1 had high loadings from the shapes of fragment and granule, and the colors of transparent, green, white and yellow, as well as moderate loadings on the shapes of foam and film. PC2 had high loadings from the shape of fiber and colors of blue and black. In summary, fragments and granules both in colors or not were the dominant apparent characteristics of microplastics.

3.1.3. Polymer type

Eleven polymer types were identified by FTIR spectroscopy, polypropylene (PP), epoxy resin (ER), polyester (PES), polymethacrylate (PMA), polyethylene (PE) and phenoxy resin (PR) being the major components. In the WP, ER was of the highest proportion with an average of 28% , followed by PP, PES, PMA and PR, whose proportions were all in the range of $13\text{--}16\%$. In the SCS, the majority of microplastics consisted of PP (31%), PE (26%) and PMA (11%), whose mean proportions were 31% , 26% and 11% , respectively. Among these major components, PP, PE and ER varied significantly different ($p < 0.05$) between the WP and SCS, indicating the polymer types of microplastics from the two areas were partly different.

The FTIR spectroscopy revealed the aging and degradation of plastics with changes in their chemical bond structures. Taking PE as an example, we compared the spectra of weathered and original PE samples, whose matching rates were 97% and 72% in the micro-FTIR analysis. As shown in Fig. 3, we found additional absorption peaks for the weathered PE, representing the hydroxyl groups ($\text{OH}, 3300\text{ cm}^{-1}$) and carbonyl groups ($\text{C=O}, 1713\text{ cm}^{-1}$). Exposed to solar UV radiation and coupled with physical abrasion, plastics would undergo photo-oxidative degradation and develop the hydroxyl groups and carbonyl groups (Singh and Sharma, 2008; Cai et al., 2018a,b). Additionally, hydroxyl and carbonyl groups were often observed in both PE and PP samples, indicating that microplastics in the SCS and WP underwent photo-oxidative degradation.

To further assess the degree of the photo-oxidative degradation, we calculated the carbonyl index for PP and PE samples. The ranges of carbonyl index values were $0.03\text{--}1.40$ (mean 0.38 ± 0.35) and $0.13\text{--}1.29$ (mean 0.70 ± 0.34) for PP and PE samples, respectively. The results for PP and PE samples were significantly different ($p < 0.05$), as many PE values were relatively higher than the PP's, revealing that PE underwent a higher degree of photo-oxidation than PP.

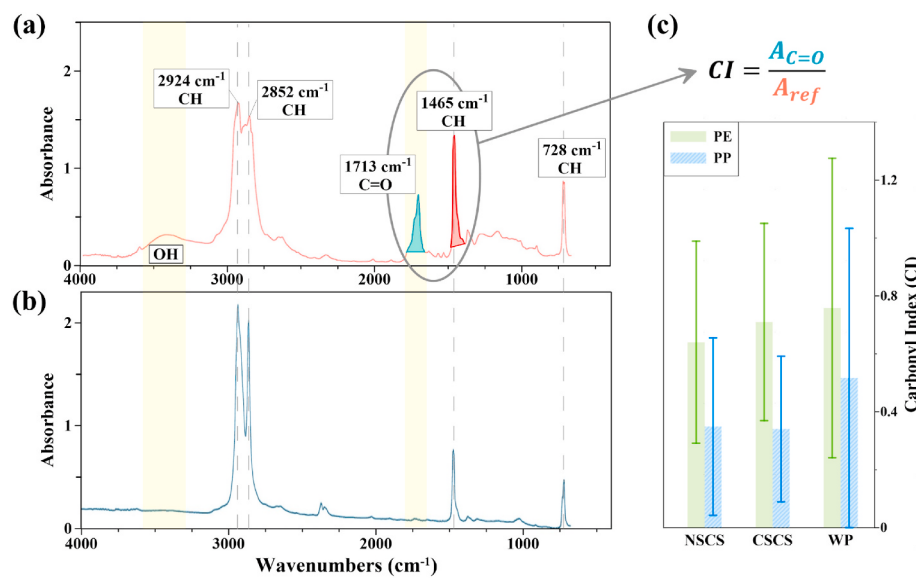


Fig. 3. FTIR spectra of weathered (a) and original (b) PE samples, and the carbonyl Index (c) of PE and PP samples collected from the northern South China Sea (NSCS), central South China Sea (CSCS), and western Pacific (WP).

3.2. Microplastic distribution and regional features

3.2.1. Spatial pattern of microplastic shapes

To discover the spatial distribution pattern, we performed a two-dimensional hierarchical cluster analysis (HCA) on microplastic shapes and the sampling sites. As shown in Fig. 4, microplastic shapes could be divided into two groups, one composed of fragment and granule, while another composed of film, foam and fiber. This classification was in accordance with the result of CA results described in section 3.1. As for the sampling sites, they could be generally categorized into three groups according to the HCA result and geography. The first group included A12, Y, S7, E130-4, E130-7, E130-12, E130-24, F2 and N18-9, and most

of these sites were located at the northern SCS or the northern part of the WP. The second group included E130-9, E130-14, E130-16 and E130-22, which were all at the south of the NEC, while the third group consisted of DC2, DC6 and H1 in the SCS. Thus, several samples from the central and northern SCS were in one cluster, while other samples from the WP and northern SCS were in another cluster.

The shape classification revealed the different environmental behaviors for microplastics with different shapes and densities. The size and shape types of microplastics were considered essential factors determining the decrease coefficients in the water column (Kooi et al., 2016). Granule and fragment are of the relatively higher densities and settling velocities, while film, foam and fiber tend to be of buoyant densities, predominantly floating and mixing at the surface layer of the oceans (Brunner et al., 2015). The spatial distribution of microplastics reflected differences between the WP and the central SCS, and the mixing effect in the northern SCS. In summer, the upper SCS is characterized by prevailing southwesterly winds and anticyclonic circulation, and could be affected by the associated eddy formation to the east of Vietnam (Gan et al., 2006). Therefore, microplastics in the WP and the central SCS represented different sources and oceanic transport processes. Those in the northern SCS showed the mixed characteristics and the similarity with those in the WP, indicating the influence of water mass mixing on microplastics, and it is further discussed in section 3.3.

3.2.2. Spatial pattern of polymer type

The PCA was performed on polymer types, and the loadings of polymer type and the scores of sample are shown in Fig. 5. Three principal components explained 66% of the variance in the data (Fig. 5), where the PC1 contributed 29% of the total variance and was heavily weighted in PP, PE and PES. PC2 contributed 23% of the total variance, heavily weighted in PMA and rayon, and PC3 contributed 14% of the total variance, heavily weighted in PR and polystyrene (PS). PP and PE were also found predominately in surface water in the literature. They are the most common types used in non-fiber plastic production, while the microplastic fibers are majorly composed of PES or acrylic (Geyer et al., 2017; Li et al., 2020). Combined with the shape proportions, we suggest the PC1 was representative for fragments and granules, and PC2 was representative for fibers. As samples from different areas were of different PCA scores, the polymer types showed spatial distinction. Compared to the particles observed in the Pacific Ocean, samples from the SCS were more likely to be with higher scores on PC1. The North

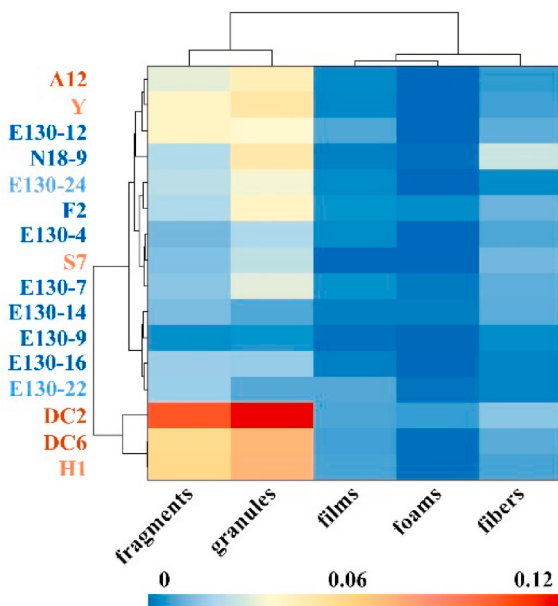


Fig. 4. Two-dimensional hierarchical cluster analysis heat map for all sampling sites and microplastic shapes. Sampling sites are labeled with different colors: western Pacific in blue (especially the equatorial Pacific sites in light blue), the northern South China Sea in orange and central South China Sea in red. (For interpretation of the references to color in this figure legend, the reader is referred to the Web version of this article.)

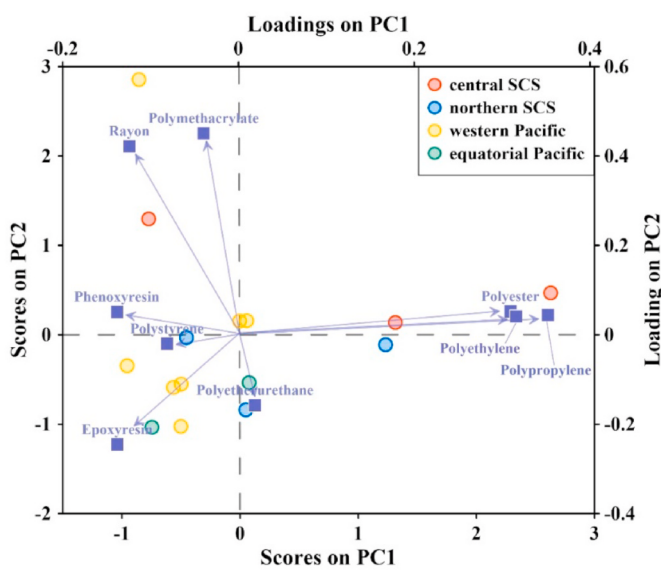


Fig. 5. Results of principal component analysis. The purple squares represent loadings of each component on PC1 and PC2. The dot shows each sample's score on PC1 and PC2, and the different colors represent different sampling areas. (For interpretation of the references to color in this figure legend, the reader is referred to the Web version of this article.)

Equatorial Counter Current influenced E130-22 and E130-24 (in green dots), and the emissions from tropical countries had high scores in both PC1 and PC2.

The average proportions of the major polymer types were plotted with their original densities, and the trends were different in the WP and the SCS (Fig. 6). In the SCS, polymers' proportions decreased with their original densities increasing. At the same time, there was no monotone decreasing trend in the WP, but showed a slight increase of proportions when their densities were near 1.2 g cm^{-3} and even higher. It is worth noting that since the saturated NaCl solution (1.20 g cm^{-3}) was used for density separation in this study, it would inevitably lead to an underestimation for some denser polymer types. Some polymers, whose original densities are higher than 1.20 g cm^{-3} , were still detected after the saturated NaCl solution separation, revealing that the physical breaking, chemical weathering and later biodegradation probably changed particles' density. For example, PVC, whose original density is 1.40 g cm^{-3} , has a density range of $1.10\text{--}1.58 \text{ g cm}^{-3}$ in marine

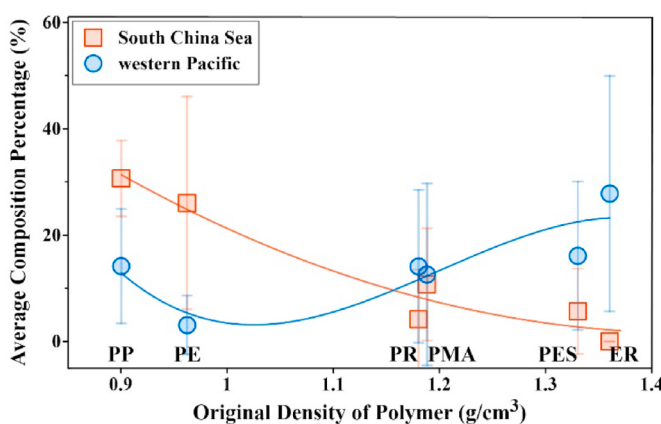


Fig. 6. The average composition percentages of polymers with different original densities. The red square is representative of data from the SCS, and the blue dot is representative for data from the WP. Density was cited from CAS database. (For interpretation of the references to color in this figure legend, the reader is referred to the Web version of this article.)

environments due to weathering, embrittlement, and biofouling (Kooi and Koelmans, 2019). It has higher sensitivity towards UV radiation, and would undergo dehydrochlorination, degrade into smaller fragments and develop carbonyl bands (C=O) during their photo-oxidation (Birer et al., 1999; Gewert et al., 2015). As shown in Fig. S3, the spectra of the field PVC sample showed additional absorption peaks approximately at 3300 cm^{-1} and 1700 cm^{-1} compared of the standard PVC. The development of hydroxyl groups and carbonyl groups revealed the oxidative degradation of PVC particles in marine environments and the possible change in their density.

In the northern SCS, the decreasing trend of proportions with polymers' densities was suggested related to the fast settling. In the water column, the density of microplastics and their biofilm stickiness determine the sink velocities, and therefore the polymer with a higher density would sink faster than the lighter plastics (Hoellein et al., 2019). Besides, the northern SCS contains a broad continental shelf, and is a relatively productive ecosystem. This will benefit the biofilm colonization, aggregation and incorporation into marine snow, thus enhancing microplastic sinking on the broad continental shelf as well (Fazey and Ryan, 2016; Hale et al., 2020). While in the WP, the variation trend of polymer proportion was quite different, which decreased firstly, then showed higher abundance with the increasing original density. As the WBC water originated from the NEC, part of the microplastics had been broken and weathered over time through various physical, chemical and biological processes (Wright et al., 2013). As shown in Fig. 3c, the average carbonyl index values for PP and PE samples from the WP were higher than those from the northern and southern SCS, reflecting that microplastics in the WP underwent a higher degree of photo-oxidation or weathering than those in the SCS.

3.3. Impact of the Kuroshio intrusion on microplastics in the SCS

3.3.1. Kuroshio fraction vs. microplastic characteristics

Water mass mixing would influence the distribution and fate of microplastics, and in the northern SCS, microplastic characteristics could reflect the impact of Kuroshio intrusion. As shown in Fig. 7a, there is a surface inflow from the WP to the northern SCS via the Luzon Strait, and the majority of Kuroshio water keeps going northward. The vertical profiles of potential temperature and salinity (T-S) in the WP, northern and central SCS were shown in Fig. 7b, generally displaying a reversed "S"-shaped T-S pattern. The water-mass properties were different between the central SCS and the WP. The SCS water tended to contain lower potential temperature and salinity than the Pacific water. The T-S patterns of the northern SCS were distributed between those of the WP and central SCS, proving the mixing process in the northern SCS.

The overall Kuroshio fractions for surface water in the northern SCS are shown in Fig. 8a. The R_K values ranged from 0.03 to 0.4 (Table S6), with the lowest value at A12 and the highest value at S7, revealing the stronger intrusion in the shelf area than in the open basin. Although the R_K value does not necessarily indicate the absolute Kuroshio fraction based on the two-end member model, it is still a statistical tool to study the response of other variables. In the northern SCS, the abundances of microplastics in various shapes showed different variation patterns with the Kuroshio fraction (Fig. 8b). Fragment, granule and foam showed a similar trend, as they increased firstly and then decreased when the fraction over 0.1, while film and fiber did not show an evident variation trend. Considering this non-monotonic trend and the original high proportions of fragment and granule in the SCS, we suggested the impact of Kuroshio on microplastics was a combination of the dilution effect and biogeochemical influence.

To further study the influence of Kuroshio intrusion on polymer types, a PCA was conducted for samples' polymer types in the northern SCS. Three principal components were obtained and contributed 33%, 20% and 12% of the total variance in the polymer types respectively, where PC1 was highly loaded in PES, PP, etc., and PC2 was highly loaded in PE and PMA (Fig. S4a). The diverse polymer types

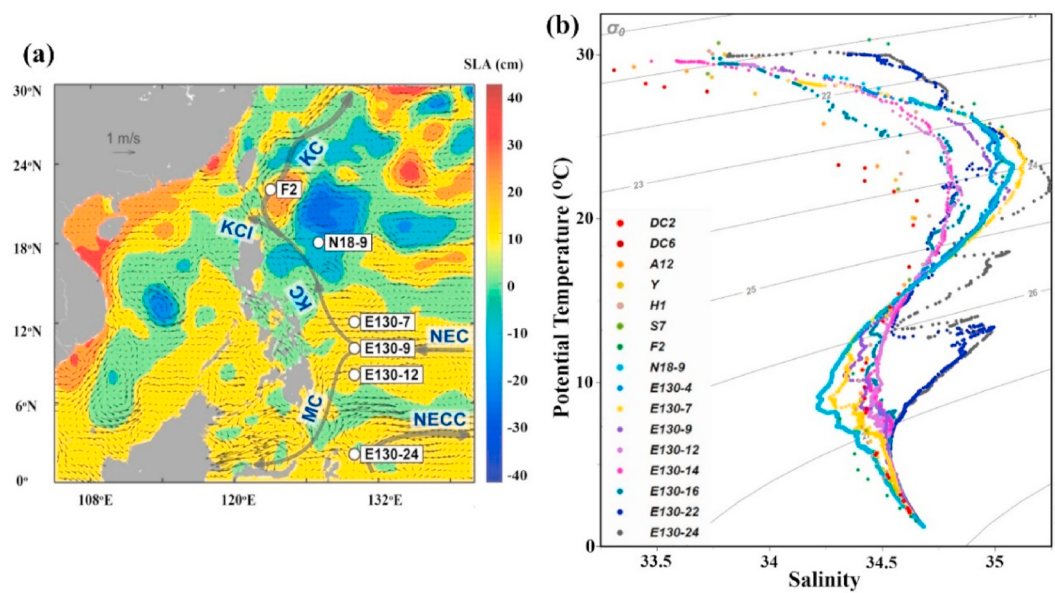


Fig. 7. Average sea surface current and sea surface height in November (a) and the potential temperature-salinity plot in these water columns (b). The data source of sea surface height and current is “AVISO + CHEMS”. November was selected as the representative month because the sampling conducted in the western Pacific was from late October to November.

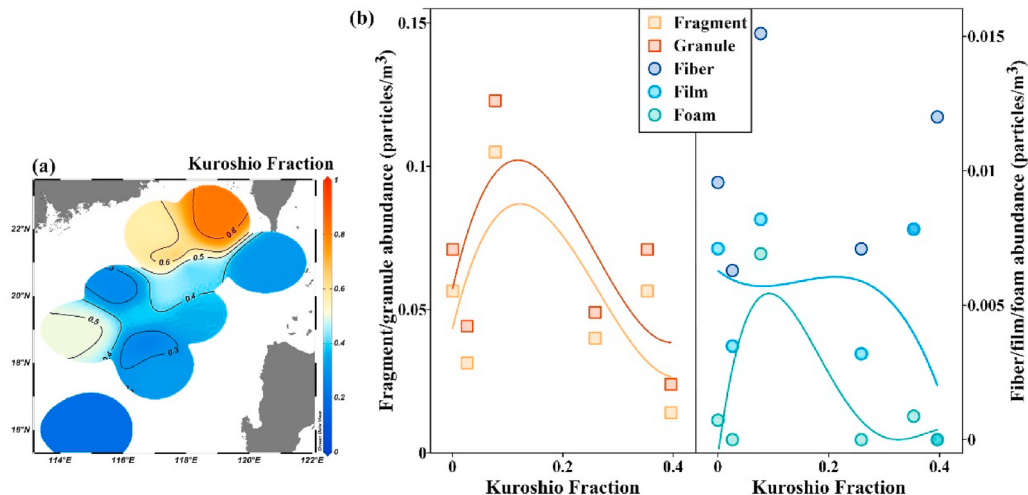


Fig. 8. Kuroshio fractions (R_K) for surface water in the northern SCS (a), and the scatter plot of microplastic abundance vs its in-situ R_K (b). Microplastics are classified based on the shape type.

microplastics in the northern SCS indicated their multiple sources, such as coastal and riverine input from land, Kuroshio intrusion, surface circulation within the SCS, and atmospheric deposition. Fig. S4b showed the sum of weighted scores of the three principal components vs. the in-situ Kuroshio fraction (R_K) at each station. The plot neither showed a linear nor monotone trend, but showed all negative values when the R_K value was larger than 0.1. Since no evident relationship was found between the complicated polymer types and Kuroshio fraction in the northern SCS, we would suggest that Kuroshio intrusion was not the dominant factor influencing the polymer types of microplastics in the northern SCS.

3.3.2. Research prospects

The Kuroshio intrusion has a seasonal variation being stronger in winter than in summer, and especially during the winter, the surface water could intrude deep into the SCS, possibly carrying microplastics to deep layers (Centurioni et al., 2004; Nan et al., 2015). The Kuroshio

takes different intruding paths, and could induce eddies and influence the horizontal advection (Yuan et al., 2006; Zhou et al., 2020). Also, the Kuroshio intrusion influences the biogeochemistry of the northern SCS, where it has a unimodal-pattern impact on microbial metabolism (Huang et al., 2019). Therefore, besides the physical mixing, the biofilm colonization and aggregation processes could be influenced by the Kuroshio intrusion. Further study is needed to discover the complicated effect of Kuroshio intrusion on the fate of microplastics.

Besides the Kuroshio current, other branches on the North Pacific WBCs play an essential role in the global distribution and oceanic circulation of microplastics. The Pacific waters are loaded with microplastics from Southeast Asia and East Asia through the KC, and part of the debris is released in the North Pacific subtropical gyre, being the Western Garbage Patch. The large-scale vortices act as conveyor belts collecting the microplastics into the Subtropical Convergence Zone, with mesoscale characteristics such as eddies in the Subtropical Frontal Zone and the Kuroshio Extension Recirculation Gyre (Howell et al., 2012).

Besides the Pacific Ocean, microplastics in the WBC system could flow to the Indian Ocean through the Indonesian Throughflow, playing a role in the return branch of the global thermohaline circulation (Hu et al., 2015). Further study is expected on the WBC system to emphasize its impact on microplastics in the ocean gyres.

4. Conclusion

Microplastic abundances in the surface water of WP were generally lower than those in the SCS, and the dominant apparent characteristics, as the shapes of fragments and granules both in colors or not, did not show significant differences between these two areas. The two-dimensional hierarchical cluster analysis results showed that fragment and granule were in the same and dominant cluster, and the related spatial classification revealed their various environmental behaviors in different areas. Fragment, granule and foam abundances showed a similar unimodal trend. They peaked when the Kuroshio fraction was 0.1, implying the effect of Kuroshio intrusion was a combination of the dilution and biogeochemical influence. The polymer compositions were complicated in the northern SCS, indicating that Kuroshio intrusion was not the dominant influencing factor. We suggest further study is needed to discover the complicated effect of Kuroshio intrusion on the fate of microplastics, and expected to extend to the WBC system.

Author statement

Mengyang Liu: Conceptualization, Writing - Original Draft. Yongcheng Ding: Data Curation. Peng Huang: Investigation. Haowen Zheng: Writing - Review & Editing. Weimin Wang: Investigation. Hongwei Ke: Funding acquisition. Fajin Chen: Visualization. Lihua Liu: Resources. Minggang Cai: Supervision.

Declaration of competing interest

The authors declare that they have no known competing financial interests or personal relationships that could have appeared to influence the work reported in this paper.

Acknowledgment

We thank all the members of the R/V *Dongfanghong II* and the R/V *Kexue* for their assistance during the research expeditions (No. 41649905, 41649909). This study was funded by the National Natural Science Foundation of China (NSFC) (41776088, U2005207), Natural Science Key Foundation of Fujian Province, China (2020J01412103), Natural Science Foundation of Fujian Province, China (2019Y4010), the Senior User Project of R/V KEXUE (KEXUE2017G09). We thank Guowen Tang, Zhai Wu, Wenxin Fan and Kaiwen Shi for their help during the sampling, Haixia He, Qianqian Wu, Renhe Chen, Xin Zhou and Xuan Ni for their assistance during the sample pretreatment, and Runqi Huang and Weiwei Fang for mapping assistance.

Appendix A. Supplementary data

Supplementary data to this article can be found online at <https://doi.org/10.1016/j.envpol.2021.117745>.

References

- Birer, O., Suzer, S., Sevil, U.A., Guven, O., 1999. UV-Vis, IR and XPS analysis of UV induced changes in PVC composites. *J. Mol. Struct.* 482–483, 515–518. [https://doi.org/10.1016/S0022-2860\(98\)00693-0](https://doi.org/10.1016/S0022-2860(98)00693-0).
- Brunner, K., Kukulka, T., Proskurowski, G., Law, K.L., 2015. Passive buoyant tracers in the ocean surface boundary layer: 2. Observations and simulations of microplastic marine debris. *J. Geophys. Res.* 120, 7559–7573. <https://doi.org/10.1002/2015jc010840>.
- Cai, M., He, H., Liu, M., Li, S., Tang, G., Wang, W., Huang, P., Wei, G., Lin, Y., Chen, B., Hu, J., Cen, Z., 2018a. Lost but can't be neglected: huge quantities of small microplastics hide in the South China Sea. *Sci. Total Environ.* 633, 1206–1216. <https://doi.org/10.1016/j.scitotenv.2018.03.197>.
- Cai, L., Wang, J., Peng, J., Wu, Z., Tan, X., 2018b. Observation of the degradation of three types of plastic pellets exposed to UV irradiation in three different environments. *Sci. Total Environ.* 628–629, 740–747. <https://doi.org/10.1016/j.scitotenv.2018.02.079>.
- Centurioni, L., Niiler, P., Lee, D.-K., 2004. Observations of inflow of Philippine sea surface water into the south China sea through the Luzon Strait. *J. Phys. Oceanogr.* 34 [https://doi.org/10.1175/1520-0485\(2004\)034<0113:OOIOPS>2.0.CO;2](https://doi.org/10.1175/1520-0485(2004)034<0113:OOIOPS>2.0.CO;2).
- Chen, B., Fan, Y., Huang, W., Rayhan, A., Chen, K., Cai, M., 2020. Observation of microplastics in mariculture water of Longjiao Bay, southeast China: influence by human activities. *Mar. Pollut. Bull.* 160, 1–8. <https://doi.org/10.1016/j.marpolbul.2020.111655>.
- Cózar, A., Echevarría, F., González-Gordillo, J.I., Irigoien, X., Úbeda, B., Hernández-León, S., Palma, Á.T., Navarro, S., García-de-Lomas, J., Ruiz, A., Fernández-de-Puelles, M.L., Duarte, C.M., 2014. Plastic debris in the open ocean. *Proc. Natl. Acad. Sci. Unit. States Am.* 111, 10239–10244. <https://doi.org/10.1073/pnas.1314705111>.
- Du, C., Liu, Z., Dai, M., Kao, K., Cao, Z., Zhang, Y., Huang, T., Wang, L., Li, Y., 2013. Impact of the Kuroshio intrusion on the nutrient inventory in the upper northern South China Sea: insights from an isopycnal mixing model. *Biogeosciences* 10 (10), 6419–6432. <https://doi.org/10.5194/bg-10-6419-2013>.
- Egger, M., Sulu-Gambari, F., Lebreton, L., 2020. First evidence of plastic fallout from the north Pacific garbage Patch. *Sci. Rep.* 10, 7495 <https://doi.org/10.1038/s41598-020-64465-8>.
- Eriksen, M., Maximenko, N., Thiel, M., Cummins, A., Lattin, G., Wilson, S., Hafner, J., Zellers, A., Rifman, S., 2013. Plastic pollution in the South Pacific subtropical gyre. *Mar. Pollut. Bull.* 68, 71–76. <https://doi.org/10.1016/j.marpolbul.2012.12.021>.
- Fazey, F.M.C., Ryan, P.G., 2016. Biofouling on buoyant marine plastics: an experimental study into the effect of size on surface longevity. *Environ. Pollut.* 210, 354–360. <https://doi.org/10.1016/j.envpol.2016.01.026>.
- Gan, J., Li, H., Curchitser, E., Haidvogel, D., 2006. Modeling South China Sea circulation: response to seasonal forcing regimes. *J. Geophys. Res.* 111 <https://doi.org/10.1029/2005JC003298>.
- Gewert, B., Plassmann, M.M., MacLeod, M., 2015. Pathways for degradation of plastic polymers floating in the marine environment. *Environ. Sci.-Proc. Imp.* 17, 1513–1521. <https://doi.org/10.1039/C5EM00207A>.
- Geyer, R., Jambeck, J.R., Law, K.L., 2017. Production, use, and fate of all plastics ever made. *Sci. Adv.* 3, e1700782 <https://doi.org/10.1126/sciadv.1700782>.
- Gigault, J., Pedrono, B., Maxit, B., Ter Halle, A., 2016. Marine plastic litter: the unanalyzed nano-fraction. *Environ. Sci.: Nano* 3, 346–350. <https://doi.org/10.1039/C6EN00008H>.
- Green, D.S., Kregting, L., Boots, B., Blockley, D.J., Brickle, P., da Costa, M., Crowley, Q., 2018. A comparison of sampling methods for seawater microplastics and a first report of the microplastic litter in coastal waters of Ascension and Falkland Islands. *Mar. Pollut. Bull.* 137, 695–701. <https://doi.org/10.1016/j.marpolbul.2018.11.004>.
- Hale, R.C., Seeley, M.E., La Guardia, M.J., Mai, L., Zeng, E.Y., 2020. A global perspective on microplastics. *J. Geophys. Res.* 125, e2018JC014719 <https://doi.org/10.1029/2018JC014719>.
- Hoellein, T.J., Shogren, A.J., Tank, J.L., Risteca, P., Kelly, J.J., 2019. Microplastic deposition velocity in streams follows patterns for naturally occurring allochthonous particles. *Sci. Rep.* 9, 3740 <https://doi.org/10.1038/s41598-019-40126-3>.
- Howell, E.A., Bograd, S.J., Morishige, C., Seki, M.P., Polovina, J.J., 2012. On North Pacific circulation and associated marine debris concentration. *Mar. Pollut. Bull.* 65, 16–22. <https://doi.org/10.1016/j.marpolbul.2011.04.034>.
- Hu, D., Wu, L., Cai, W., Gupta, A.S., Ganachaud, A., Qiu, B., Gordon, A.L., Lin, X., Chen, Z., Hu, S., Wang, G., Wang, Q., Sprintall, J., Qu, T., Kashino, Y., Wang, F., Kessler, W.S., 2015. Pacific western boundary currents and their roles in climate. *Nature* 522, 299–308. <https://doi.org/10.1038/nature14504>.
- Huang, Y., Laws, E., Chen, B., Huang, B., 2019. Stimulation of heterotrophic and autotrophic metabolism in the mixing Zone of the Kuroshio current and northern South China sea: implications for export production. *J. Geophys. Res.* 124 <https://doi.org/10.1029/2018JC004833>.
- Imawaki, S., Uchida, H., Ichikawa, H., Fukasawa, M., Umatani, S.-i., Group, t.A., 2001. Satellite altimeter monitoring the Kuroshio Transport south of Japan. *Geophys. Res. Lett.* 28, 17–20. <https://doi.org/10.1029/2000gl011796>.
- Jambeck, J.R., Geyer, R., Wilcox, C., Siegler, T.R., Perryman, M., Andrady, A., Narayan, R., Law, K.L., 2015. Marine pollution. Plastic waste inputs from land into the ocean. *Science* 347, 768–771. <https://doi.org/10.1126/science.1260352>.
- Kooi, M., Koelmans, A.A., 2019. Simplifying microplastic via continuous probability distributions for size, shape, and density. *Environ. Sci. Technol. Lett.* 6, 551–557. <https://doi.org/10.1021/acs.estlett.9b00379>.
- Kooi, M., Reisser, J., Slat, B., Ferrari, F.F., Schmid, M.S., Cunsolo, S., Brambini, R., Noble, K., Sirks, L.A., Linders, T.E., Schoeneich-Argent, R.J., Koelmans, A.A., 2016. The effect of particle properties on the depth profile of buoyant plastics in the ocean. *Sci. Rep.* 6, 33882 <https://doi.org/10.1038/srep33882>.
- Law, K.L., Morét-Ferguson, S.E., Goodwin, D.S., Zettler, E.R., DeForce, E., Kukulka, T., Proskurowski, G., 2014. Distribution of surface plastic debris in the Eastern Pacific Ocean from an 11-year data set. *Environ. Sci. Technol.* 48, 4732–4738. <https://doi.org/10.1021/es4053076>.
- Lebreton, L.C.M., van der Zwet, J., Damsteeg, J.W., Slat, B., Andrady, A., Reisser, J., 2017. River plastic emissions to the world's oceans. *Nat. Commun.* 8, 15611 <https://doi.org/10.1038/ncomms15611>.
- Li, D., Liu, K., Li, C., Peng, G., Andrady, A.L., Wu, T., Zhang, Z., Wang, X., Song, Z., Zong, C., Zhang, F., Wei, N., Bai, M., Zhu, L., Xu, J., Wu, H., Wang, L., Chang, S., Zhu, W., 2020. Profiling the vertical transport of microplastics in the West Pacific

- Ocean and the East Indian Ocean with a novel in situ filtration technique. Environ. Sci. Technol. 54, 12979–12988. <https://doi.org/10.1021/acs.est.0c02374>.
- Liu, M., Zheng, H., Wang, W., Ke, H., Huang, P., Liu, S., Chen, F., Lin, Y., Cai, M., 2021. Enhanced sinks of polycyclic aromatic hydrocarbons due to Kuroshio intrusion: implications on biogeochemical processes in the ocean-dominated marginal seas. Environ. Sci. Technol. 55, 6838–6847. <https://doi.org/10.1021/acs.est.1c01009>.
- Lusher, A.L., Tirelli, V., O'Connor, I., Officer, R., 2015. Microplastics in Arctic polar waters: the first reported values of particles in surface and sub-surface samples. Sci. Rep. 5, 14947 <https://doi.org/10.1038/srep14947>.
- Mai, L., Bao, L.-J., Shi, L., Liu, L.-Y., Zeng, E.Y., 2018. Polycyclic aromatic hydrocarbons affiliated with microplastics in surface waters of Bohai and Huanghai Seas, China. Environ. Pollut. 241, 834–840. <https://doi.org/10.1016/j.envpol.2018.06.012>.
- Mai, L., Sun, X.F., Xia, L.L., Bao, L.J., Liu, L.Y., Zeng, E.Y., 2020. Global riverine plastic outflows. Environ. Sci. Technol. 54, 10049–10056. <https://doi.org/10.1021/acs.est.0c02273>.
- Mai, L., You, S.N., He, H., Bao, L.J., Liu, L.Y., Zeng, E.Y., 2019. Riverine microplastic pollution in the Pearl River Delta, China: are modeled estimates accurate? Environ. Sci. Technol. 53, 11810–11817. <https://doi.org/10.1021/acs.est.9b04838>.
- Mountford, A.S., Morales Maqueda, M.A., 2019. Eulerian Modeling of the three-dimensional distribution of seven popular microplastic types in the global ocean. J. Geophys. Res. 124, 8558–8573. <https://doi.org/10.1029/2019jc015050>.
- Mu, J., Zhang, S., Qu, L., Jin, F., Fang, C., Ma, X., Zhang, W., Wang, J., 2019. Microplastics abundance and characteristics in surface waters from the Northwest Pacific, the Bering Sea, and the Chukchi Sea. Mar. Pollut. Bull. 143, 58–65. <https://doi.org/10.1016/j.marpolbul.2019.04.023>.
- Nan, F., Xue, H., Yu, F., 2015. Kuroshio intrusion into the south China sea: a review. Prog. Oceanogr. 137, 314–333. <https://doi.org/10.1016/j.pocean.2014.05.012>.
- Pan, Z., Liu, Q., Sun, Y., Sun, X., Lin, H., 2019. Environmental implications of microplastic pollution in the Northwestern Pacific Ocean. Mar. Pollut. Bull. 146, 215–224. <https://doi.org/10.1016/j.marpolbul.2019.06.031>.
- Poulain, M., Mercier, M.J., Brach, L., Martignac, M., Routaboul, C., Perez, E., Desjean, M.C., Ter Halle, A., 2019. Small microplastics as a main contributor to plastic mass balance in the North Atlantic Subtropical Gyre. Environ. Sci. Technol. 53, 1157–1164. <https://doi.org/10.1021/acs.est.8b05458>.
- Qiu, B., Chen, S., 2005. Variability of the Kuroshio Extension jet, recirculation gyre, and mesoscale eddies on decadal time scales. J. Phys. Oceanogr. 35 <https://doi.org/10.1175/JPO2807.1>.
- Qiu, B., Miao, W., 2000. Kuroshio path variations south of Japan: bimodality as a self-sustained internal oscillation. J. Phys. Oceanogr. 30, 2124–2137. [https://doi.org/10.1175/1520-0485\(2000\)030<2124:Kpvsj>2.0.Co;2](https://doi.org/10.1175/1520-0485(2000)030<2124:Kpvsj>2.0.Co;2).
- Schlining, K., von Thun, S., Kuhnz, L., Schlining, B., Lundsten, L., Jacobsen Stout, N., Chaney, L., Connor, J., 2013. Debris in the deep: using a 22-year video annotation database to survey marine litter in Monterey Canyon, central California, USA. Deep Sea Res., Part I 79, 96–105. <https://doi.org/10.1016/j.dsr.2013.05.006>.
- Schönlau, C., Karlsson, T.M., Rotander, A., Nilsson, H., Engwall, M., van Bavel, B., Kärrman, A., 2020. Microplastics in sea-surface waters surrounding Sweden sampled by manta trawl and in-situ pump. Mar. Pollut. Bull. 153, 111019 <https://doi.org/10.1016/j.marpolbul.2020.111019>.
- Singh, B., Sharma, N., 2008. Mechanistic implications of plastic degradation. Polym. Degrad. Stabil. 93, 561–584. <https://doi.org/10.1016/j.polymdegradstab.2007.11.008>.
- Sterl, M.F., Delandmeter, P., van Sebille, E., 2020. Influence of barotropic tidal currents on transport and accumulation of floating microplastics in the global open ocean. J. Geophys. Res. 125, e2019JC015583 <https://doi.org/10.1029/2019jc015583>.
- Sun, C., Ding, J., Gao, F., 2021. Methods for Microplastic Sampling and Analysis in the Seawater and Fresh Water Environment. Method. Enzymol. Academic Press. <https://doi.org/10.1016/bs.mie.2020.12.009>.
- Sussarellu, R., Suquet, M., Thomas, Y., Lambert, C., Fabiou, C., Pernet, M.E.J., Le Goic, N., Quillien, V., Mingant, C., Epelboin, Y., Corporeau, C., Guyomarch, J., Robbens, J., Paul-Pont, I., Soudant, P., Huvet, A., 2016. Oyster reproduction is affected by exposure to polystyrene microplastics. Proc. Natl. Acad. Sci. Unit. States Am. 113, 2430–2435. <https://doi.org/10.1073/pnas.1519019113>.
- Tang, G., Liu, M., Zhou, Q., He, H., Chen, K., Zhang, H., Hu, J., Huang, Q., Luo, Y., Ke, H., Chen, B., Xu, X., Cai, M., 2018. Microplastics and polycyclic aromatic hydrocarbons (PAHs) in Xiamen coastal areas: implications for anthropogenic impacts. Sci. Total Environ. 634, 811–820. <https://doi.org/10.1016/j.scitotenv.2018.03.336>.
- Waller, C.L., Griffiths, H.J., Waluda, C.M., Thorpe, S.E., Loaiza, I., Moreno, B., Pacherres, C.O., Hughes, K.A., 2017. Microplastics in the Antarctic marine system: an emerging area of research. Sci. Total Environ. 598, 220–227. <https://doi.org/10.1016/j.scitotenv.2017.03.283>.
- Wang, C., Guo, W., Li, Y., Stubbins, A., Li, Y., Song, G., Wang, L., Cheng, Y., 2017. Hydrological and Biogeochemical Controls on Absorption and Fluorescence of Dissolved Organic Matter in the Northern South China Sea. Journal of Geophysical Research: Biogeosciences 122 (12), 3405–3418. <https://doi.org/10.1002/2017jg004100>.
- Wang, T., Zou, X., Li, B., Yao, Y., Zang, Z., Li, Y., Yu, W., Wang, W., 2019. Preliminary study of the source apportionment and diversity of microplastics: taking floating microplastics in the South China Sea as an example. Environ. Pollut. 245, 965–974. <https://doi.org/10.1016/j.envpol.2018.10.110>.
- Wichmann, D., Delandmeter, P., van Sebille, E., 2019. Influence of near-surface currents on the global dispersal of marine microplastic. J. Geophys. Res. 124, 6086–6096. <https://doi.org/10.1029/2019jc015328>.
- Wright, S.L., Thompson, R.C., Galloway, T.S., 2013. The physical impacts of microplastics on marine organisms: a review. Environ. Pollut. 178, 483–492. <https://doi.org/10.1016/j.envpol.2013.02.031>.
- Wu, K., Dai, M., Chen, J., Meng, F., Li, X., Liu, Z., Du, C., Gan, J., 2015. Dissolved organic carbon in the South China Sea and its exchange with the Western Pacific Ocean. Deep Sea Res. Part II: Topical Stud. Oceanogr. 122, 41–51. <https://doi.org/10.1016/j.dsr2.2015.06.013>.
- Xia, B., Sui, Q., Sun, X., Zhu, L., Wang, R., Cai, M., Chen, B., Qu, K., 2021. Microplastic pollution in surface seawater of Sanggou Bay, China: occurrence, source and inventory. Mar. Pollut. Bull. 162, 111899 <https://doi.org/10.1016/j.marpolbul.2020.111899>.
- Yuan, D., Han, W., Hu, D., 2006. Surface Kuroshio path in the Luzon Strait area derived from satellite remote sensing data. J. Geophys. Res. 111 <https://doi.org/10.1029/2005JC003412>.
- Zhang, Z., Wu, H., Peng, G., Xu, P., Li, D., 2020. Coastal ocean dynamics reduce the export of microplastics to the open ocean. Sci. Total Environ. 713, 136634 <https://doi.org/10.1016/j.scitotenv.2020.136634>.
- Zhao, W., Huang, W., Yin, M., Huang, P., Ding, Y., Ni, X., Xia, H., Liu, H., Wang, G., Zheng, H., Cai, M., 2020. Tributary inflows enhance the microplastic load in the estuary: a case from the Qiantang River. Mar. Pollut. Bull. 156, 111152 <https://doi.org/10.1016/j.marpolbul.2020.111152>.
- Zhou, K., Dai, M., Xiu, P., Wang, L., Hu, J., Benitez-Nelson, C.R., 2020. Transient enhancement and decoupling of carbon and opal export in cyclonic eddies. J. Geophys. Res. 125, e2020JC016372 <https://doi.org/10.1029/2020JC016372>.